Journal of Alloys and Compounds 509 (2011) 2572–2575

Contents lists available at ScienceDirect

Journal of Alloys and Compounds

journal homepage: www.elsevier.com/locate/jallcom

Electrochemical effect of AB_3 alloy on CoB alloy in CoB-x wt.% AB_3 mixture electrodes

Dawei Song [b], Yijing Wang [a,*], Yaping Wang [a], Qinghong Wang [a], Li Li [a], Yan Han [a], Lifang Jiao [a], Shumin Han [c], Huatang Yuan [a]

[a] Institute of New Energy Material Chemistry, Key Laboratory of Advanced Energy Materials Chemistry (MOE), Nankai University, Tianjin 300071, PR China
[b] School of Chemistry and Chemical Engineering, Henan University of Technology, Zhengzhou 450001, PR China
[c] State Key Laboratory of Metastable Materials Science and Technology, Yanshan University, Qinhuangdao 066004, PR China

ARTICLE INFO

Article history:
Received 9 March 2010
Received in revised form
11 November 2010
Accepted 15 November 2010
Available online 23 November 2010

Keywords:
Electrode materials
Powder metallurgy
Electrochemical reactions
X-ray diffraction

ABSTRACT

CoB alloy prepared by arc melting possesses excellent cyclic stability but low discharge capacity, while AB_3 hydrogen storage alloy prepared by inductive melting exhibits high discharge capacity but poor cyclic stability as negative electrode materials of alkaline rechargeable nickel-based batteries. A series of CoB-x wt.% AB_3 mixtures were synthesized by simple mixing of CoB alloy powders and AB_3 alloy powders. Electrochemical measurements revealed that the reversible discharge capacity and cycle stability of the mixture electrodes were largely improved, compared with CoB alloy electrode and AB_3 alloy electrode. The CoB-x wt.% AB_3 (x = 20) electrode displays the highest discharge capacity of the 40th cycle and the CoB-x wt.% AB_3 (x = 10) electrode displays the highest discharge capacity of the 100th cycle among all the mixture electrodes. The electrochemical effect of AB_3 alloy on CoB alloy in mixture electrodes was also systematically investigated.

1. Introduction

Recently, Co-B alloy has attracted increasing attention as a negative electrode material of alkaline rechargeable nickel-based batteries [1–7]. And much progress has been made to improve its discharge capacity in alkaline electrolyte [8–10]. Han et al. prepared Co-B-Si alloys with and obtained a discharge capacity of 270 mAh g^{-1} after 100 cycles [11]. Lu et al. introduced sulfur into the Co-B-S system and the electrochemical properties of the Co-B alloys were greatly improved [12]. In our previous work, we prepared Co-B alloy by annealing the products of chemical reduction method, and obtained a capacity of 400 mAh g^{-1} [13]. It is obvious that the introduction of some dissoluble compositions, which could enlarge the contact area of Co-B with alkaline electrolyte may have effect on the improvement of the Co-B alloys.

It is well known that AB_3 type R-Mg-Ni system hydrogen storage alloys have been intensively studied as one of the most promising negative electrode candidates for Ni-MH secondary batteries [14–17]. However, AB_3 hydrogen storage alloys have higher discharge capacities but lower cyclic stabilities. Although there has been a lot of work to improve the cyclic stability of these alloys in recent years, they are still far from commercial requirements [18–20].

In order to get a kind of material with high discharge capacity and excellent cyclic stability, a series of CoB-x wt.% AB_3 mixtures were synthesized and electrochemically used as anode materials for alkaline rechargeable nickel-based battery. The electrochemical effect of AB_3 alloy on CoB alloy in mixture electrodes are discussed.

2. Experimental

2.1. Synthesis

CoB alloy and AB_3 ($La_{0.80}Mg_{0.20}Ni_{2.4}Mn_{0.10}Co_{0.55}Al_{0.10}$) alloy were prepared by arc melting and inductive melting, respectively. The two alloy ingots were mechanically crushed to powders, and then CoB-x wt.% AB_3 (x = 10, 20, 30, 40, 50, 60) mixtures were synthesized by simple mixing of CoB powders and AB_3 powders at different ratios and ground with a mortar.

2.2. Characterization

The structures of mixtures were characterized by powder X-ray diffraction (Rigaku DMax-2500, Cu Kα radiation, graphite monochromator).

Powder X-ray photoelectron spectra (XPS) measurements were performed on Kratos Axis Ultra system, employing a monochromatic Al-Kα X-ray source ($h\nu$ = 1486.6 eV), hybrid (magnetic/electrostatic) optics and a multi-channel plate and delay line detector (DLD).

* Corresponding author. Tel.: +86 22 23503639; fax: +86 22 23503639.
E-mail address: wangyj@nankai.edu.cn (Y. Wang).

0925-8388/$ – see front matter.
doi:10.1016/j.jallcom.2010.11.092

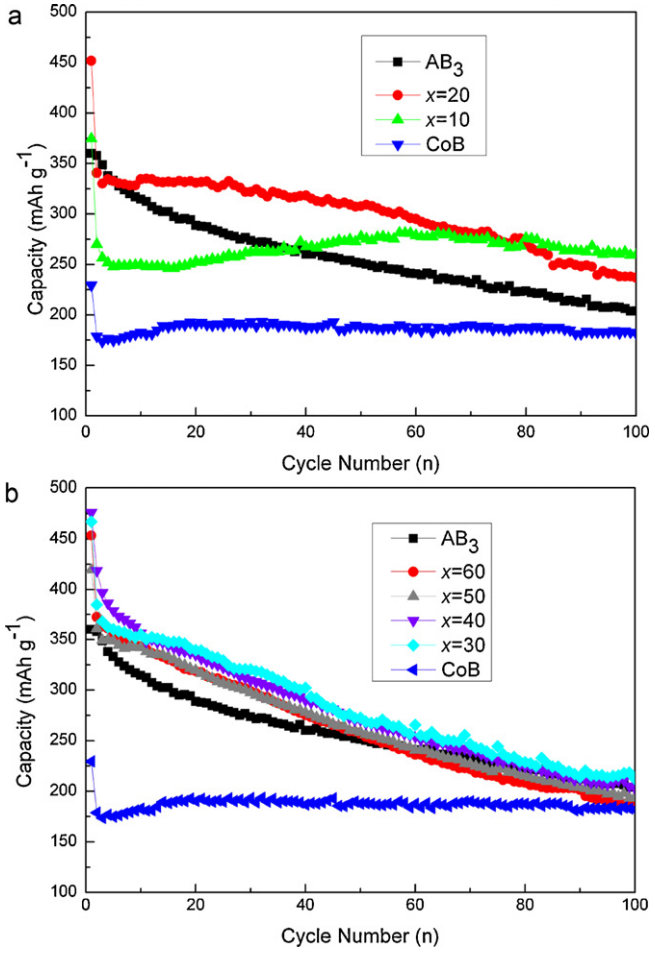

Fig. 1. The cycle stability curves of CoB alloy, AB_3 alloy and CoB-*x* wt.% AB_3 mixtures electrodes.

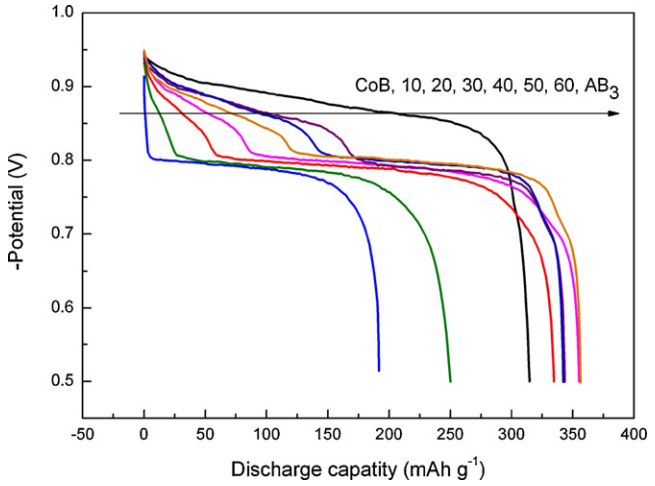

Fig. 2. The 10th cycle discharge curves of CoB alloy, AB_3 alloy and CoB-*x* wt.% AB_3 mixtures electrodes.

2.3. Electrochemical measurements

The electrodes for test were prepared as follows: 0.8 g of the mixture of as-prepared powder and nickel powder (mass ratio 1:3) was pressed into pellet (10 mm in diameter) at 30 MPa. A sandwich of the pellet between two foam nickel disks (20 mm in diameter) was pressed at 10 MPa, on which a nickel strip was soldered.

Electrochemical measurements were conducted in a three-compartment cell using a Land battery test instrument. $NiOOH/Ni(OH)_2$ and Hg/HgO were used as the counter electrode and the reference electrode, respectively. In each charge–discharge cycle test, the negative electrode was charged for 6 h at 100 mA g^{-1} and discharged at 25 mA g^{-1} up to the cut-off voltage set at −0.5 V (vs. Hg/HgO). The electrolyte solution was a 6 M KOH aqueous solution. The interval between charge and discharge was 5 min. Zahner IM6e electrochemical workstation was used for cyclic voltammetry (CV) (scan rate: 0.2 mV s^{-1}, −1.2 to −0.4 V vs. Hg/HgO). All the experiments were conducted at room temperature.

3. Results and discussion

3.1. Electrochemical performance

Fig. 1 shows the cycle stability curves of CoB alloy, AB_3 alloy and CoB-*x* wt.% AB_3 mixtures electrodes at a current density of 25 mA g^{-1}. It shows that the cycle stability of CoB-*x* wt.% AB_3 mixture electrode is improved. As shown in Fig. 1a, CoB alloy electrode has an excellent cyclic stability but low discharge capacities, while AB_3 alloy electrode displays higher discharge capacities but a poor cyclic stability. Therefore, we conclude that the cycle curves of CoB-*x* wt.% AB_3 mixture electrodes vary with the mass content of AB_3 alloy. According to the specific information given in Fig. 1b and Table 1, the maximum discharge capacity of CoB-*x* wt.% AB_3 ($x = 40$) mixture electrode reaches 476.2 mAh g^{-1}. The CoB-*x* wt.% AB_3 ($x = 20$) electrode displays the highest discharge capacity of the 40th cycle and the CoB-*x* wt.% AB_3 ($x = 10$) electrode displays the highest discharge capacity of the 100th cycle among all the mixtures electrodes, which are much higher than pure CoB alloy electrode and pure AB_3 alloy electrode. Among all the mixtures electrodes, CoB-*x* wt.% AB_3 ($x = 10$) mixture electrode displays the best cycle stability ($C_{100th}/C_{40th}\% = 96.86\%$), which is close to that of pure CoB alloy electrode ($C_{100th}/C_{40th}\% = 97.38\%$). By comparing the discharge capacities of the 40th and 100th cycles and the results of $C_{100th}/C_{40th}\%$, the electrodes with less AB_3 alloy exhibit better cycle stabilities in the charge–discharge process. This is because the CoB alloy dominates the cycle performance of the electrodes.

The 10th cycle discharge curves of CoB alloy, AB_3 alloy and CoB-*x* wt.% AB_3 mixtures electrodes are compared in Fig. 2. There are two potential plateaus in each mixtures electrode curve. The first potential plateau at −0.87 V (vs. Hg/HgO) can be attributed to AB_3 alloy, and the second potential plateau at −0.78 V (vs. Hg/HgO) is positively related to CoB alloy. When the mass content of AB_3 is 20%, the discharge capacity of the first potential plateau is exact 20% of pure AB_3 alloy electrode, but that of the second potential plateau is higher than 80% of pure CoB alloy electrode. The similar results can also be found in other CoB-*x* wt.% AB_3 mixture electrodes. Consequently, the increased discharge capacity of CoB in CoB-*x* wt.% AB_3 mixture electrodes is the reason that the mixtures electrodes have higher discharge capacity.

Table 1
Cycle stability of CoB, AB_3 alloy and CoB-*x* wt.% AB_3 mixtures electrodes.

	CoB	$x = 10$	$x = 20$	$x = 30$	$x = 40$	$x = 50$	$x = 60$	AB_3
C_{1st}	229.5	374.7	451.9	467.2	476.1	419.5	453.5	360.0
C_{40th}	186.8	267.7	318.4	302.4	290.2	278.0	275.0	260.2
C_{100th}	181.9	259.3	237.0	212.4	203.3	194.2	185.5	204.0
$C_{100th}/C_{40th}\%$	97.38	96.86	74.44	70.24	70.06	69.86	67.45	78.40

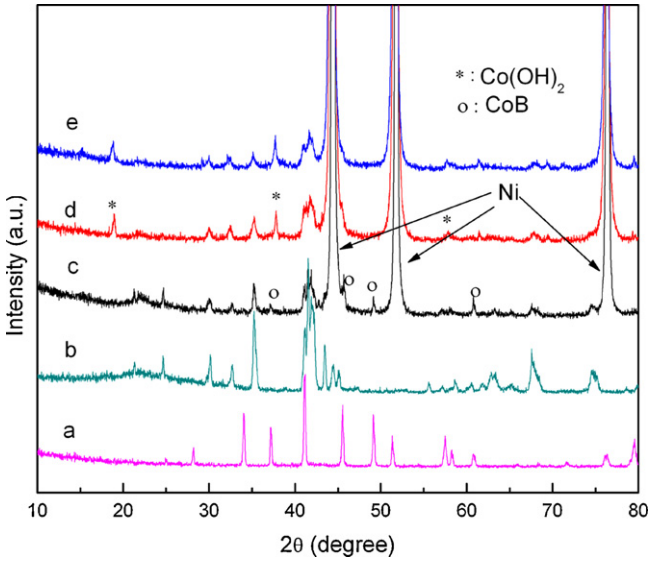

Fig. 3. XRD patterns of CoB-*x* wt.% AB_3 (x = 50) mixture: (a) CoB alloy, (b) AB_3 alloy, (c) CoB-*x* wt.% AB_3 (x = 50) mixture, (d) CoB-*x* wt.% AB_3 (x = 50) mixture electrode after the 1st cycle, (e) CoB-*x* wt.% AB_3 (x = 50) mixture electrode after the 2nd cycle.

3.2. Material characterization

To further investigate the effect of AB_3 alloy on CoB alloy, XRD patterns of CoB-*x* wt.% AB_3 (x = 50) mixture are showed in Fig. 3. Three Ni peaks are attributed to the doped Ni powder in electrode. The main phases of AB_3 alloy are $LaNi_3$ phase and $LaNi_5$ phase, and the main phase of CoB alloy is CoB phase. The similar diffractions are observed in CoB-*x* wt.% AB_3 (x = 50) mixture. After the 1st charge–discharge cycle, CoB peaks disappear and $Co(OH)_2$ peaks appear. After the 2nd cycle, the intensity of $Co(OH)_2$ peaks increases, while those of AB_3 alloy have little change. However, which is eroded to $Co(OH)_2$, the whole CoB alloy or only those on the surface?

XPS spectra of CoB alloy with Co 2p are shown to explain the above question (Fig. 4). In the initial alloy, Co 2p peak appears at 778.3 eV, indicating that the Co exists in the form of CoB. After the 1st cycle, a peak appears at 780 eV and only a small Co 2p peak appears at 778.3 eV, indicating that most CoB turns to $Co(OH)_2$ on the surface. After the 2nd cycle, there is only one peak appearing at 780 eV. It indicates that all CoB transforms to be $Co(OH)_2$ on the

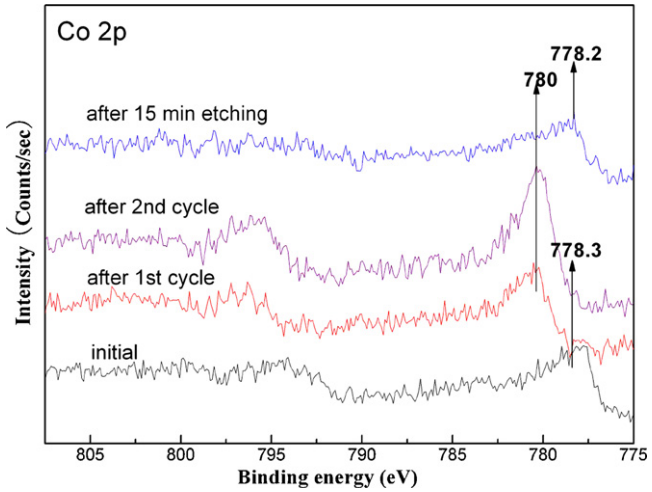

Fig. 4. XPS spectra of CoB alloy with Co 2p.

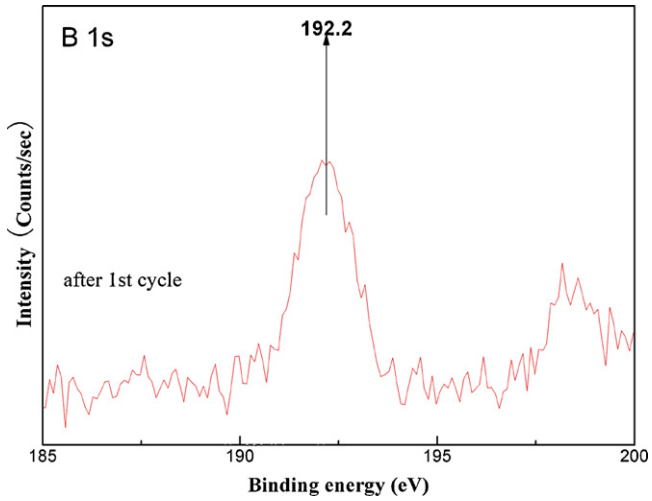

Fig. 5. XPS spectra of CoB alloy with B 1s.

electrode surface. However, after etched for 15 min, there is Co 2p peak appearing at 778.2 eV, showing that most Co inside the alloy still exists in metallic state. There is also Co 2p peak at 780 eV can be found, indicating that only a little Co inside the alloy has been eroded. In this case, the $Co(OH)_2$ exist as on the surface of the alloy during charge–discharge process and CoB is still the main phase inside the alloy.

Fig. 5 shows the XPS spectra of CoB alloy with B 1s after the 1st cycle. The B 1s peak appearing at around 192.2 eV, indicates the existence of B_2O_3. And specially, no peak of B in 0 oxidation can be found (including B in CoB or B element, at about 188 eV).

In the previous study [21], a charge–discharge mechanism of CoB alloy was proposed. In the discharge process, firstly, B and Co on the surface are oxidized in the KOH solution, all the boron is oxidized to form B_2O_3, Co is oxidized to form $Co(OH)_2$ film on the surface of the CoB. Secondly, all the B_2O_3 and part of the $Co(OH)_2$ on the surface dissolves gradually into the KOH solution. Thirdly, the dissolution creates the new surface inside the alloy. The KOH solution comes into and reacts on the new surface. And the above reaction occurs again. It forms a full loop. And the charge reaction is the transformation from $Co(OH)_2$ to Co.

The whole charge–discharge reaction can be expressed as the faradaic redox mechanism.

$$Co + 2OH^- \underset{\text{charge}}{\overset{\text{discharge}}{\rightleftarrows}} Co(OH)_2 + 2e \quad (1)$$

So the discharge capacity of CoB alloy is due to the faradaic redox transformation of $Co(OH)_2$/Co on the surface, and inner CoB contributes little.

3.3. Cyclic voltammetry test

Fig. 6 shows the cyclic voltammetry (CV) curves of AB_3 alloy, CoB alloy and CoB-*x* wt.% AB_3 (x = 10, 20, 60) mixture electrodes. The curve shape and peak voltage of CoB alloy electrode are different from those of AB_3 alloy electrode. A pair of obvious redox peaks is detected in CoB alloy electrode curve, confirming that the reversible capacity is mainly based on the faradaic redox reaction. While AB_3 alloy electrode displays wide oxidation peak and unconspicuous reduction peak, which are the typical feature of absorbtion–desorption hydrogen reaction. It is observed that the oxidation peaks of the CoB-*x* wt.% AB_3 mixture electrodes widen with the increase of AB_3 alloy and the reduction peaks shift positively. The CV curve of CoB-*x* wt.% AB_3 (x = 10, 20, 60) mixture electrode resembles that of CoB alloy electrode and that of AB_3 alloy

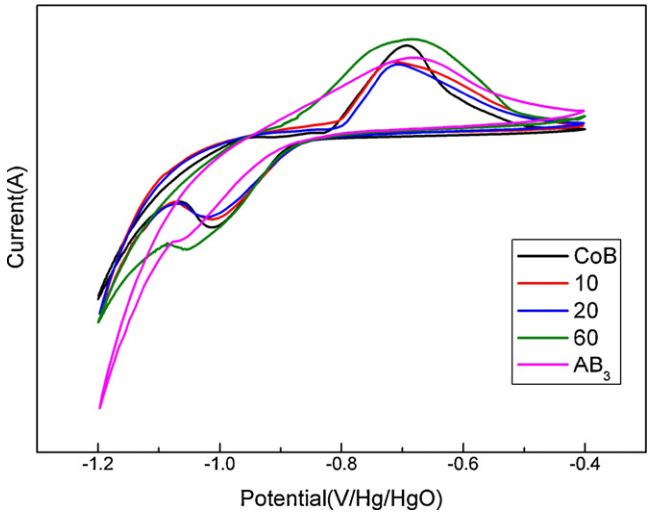

Fig. 6. Cyclic voltammetry (CV) curves of AB_3 alloy, CoB alloy and CoB-*x* wt.% AB_3 (*x* = 10, 20, 60) mixtures electrodes.

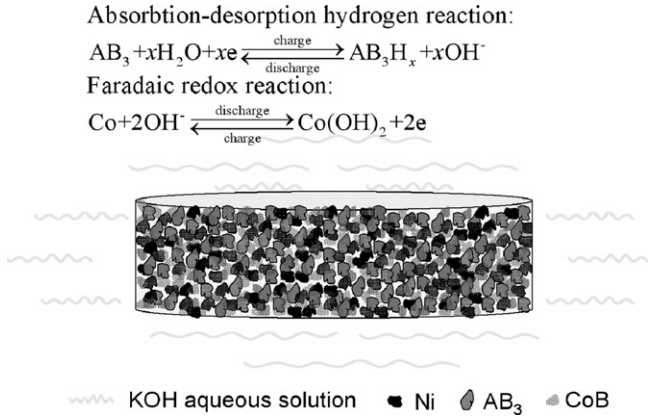

Scheme 1. The function schematic representation of AB_3 alloy on CoB alloy in mixture electrodes.

electrode, indicating that both the absorbtion–desorption hydrogen reaction and the faradaic redox reaction occur in CoB-*x* wt.% AB_3 mixtures electrode, during the charge–discharge process.

Similar to CoB alloy electrode, the charge–discharge reaction of pure Co powder electrode is also faradaic redox reaction. The discharging capacity of Co potential plateau also increases after mixing with AB_3 alloy.

3.4. Function mechanism of AB_3 alloy on CoB alloy

Based on the above analysis, both the absorbtion–desorption hydrogen reaction of AB_3 alloy and the faradaic redox reaction of CoB alloy exist during the charge–discharge process of CoB-*x* wt.% AB_3 mixture electrodes. For CoB alloy, the discharge capacity is intimately dependent on the utilization of the active material, which is largely influenced by the contact area between CoB and alkaline solution. According to our previous work [21], the possible function mechanism of AB_3 alloy on CoB alloy in mixture electrodes can be schematically shown in Scheme 1. As-prepared AB_3 alloy particles and CoB alloy particles are both irregular massive, so the CoB-*x* wt.% AB_3 mixture electrodes possess lots of interspaces. In the process of electrode preparation, the interspaces could not be removed, resulting in large surface areas of CoB alloy. During the charge–discharge process, the interspaces are impregnated with alkaline solution and increase the contact area between CoB alloy particles and alkaline solution, which is in favor of the surface electrochemical redox to improve the capacity utilization. In addition, the addition of AB_3 alloy particles leads to well dispersion of CoB alloy particles. Thus, the discharge capacity of CoB alloy is largely enhanced.

4. Conclusions

A series of CoB-*x* wt.% AB_3 mixtures are synthesized by simple mixing of CoB alloy powders and AB_3 alloy powders. The mixture electrodes display high discharge capacities and good cycle stability. The discharge capacities are attributed to the absorbtion–desorption hydrogen reaction of AB_3 alloy and the faradaic redox reaction of CoB alloy. The possible function mechanism of AB_3 alloy on CoB alloy in mixture electrode is proposed. This discovery provides a new way to improve electrochemical properties of CoB negative electrode of alkaline rechargeable Ni-based batteries.

Acknowledgements

This work was financially supported by the National High-Tech Research and Development Program of China (No. 2007AA05Z149 and 2007AA05Z108), the Major State Basic Research Development Program of China (No. 2010CB631303), the National Natural Science Foundation of China (No. 50631020, 50701025, and 50971071), the Doctoral Foundation of Ministry of Education of China (No. 20070055064), MOE Innovation Team (IRT0927).

References

[1] Y. Liu, Y.J. Wang, L.L. Xiao, D.W. Song, Y.P. Wang, L.F. Jiao, H.T. Yuan, Electrochim. Acta 53 (2008) 2265.
[2] Y.D. Wang, X.P. Ai, H.X. Yang, Chem. Mater. 16 (2004) 5194.
[3] Y.D. Wang, X.P. Ai, Y.L. Cao, H.X. Yang, Electrochem. Commun. 6 (2004) 780.
[4] D.S. Lu, W.S. Li, X. Jiang, C.L. Tan, R.H. Zeng, J. Alloys Compd. 485 (2009) 621.
[5] C. Wu, Y. Bai, F. Wu, L.W. Dong, X. Wang, L.X. Yang, C.Z. Zhang, Electrochim. Acta 53 (2008) 4715.
[6] D.S. Lu, W.S. Li, F.M. Xiao, R.H. Tang, Electrochem. Commun. 12 (2010) 362.
[7] C. Wu, Y. Bai, F. Wu, X. Wang, J.Y. Lu, C. Qiao, Electrochem. Commun. 11 (2009) 2173.
[8] C. Wu, Y. Bai, X. Wang, F. Wu, C.Z. Zhang, Solid State Ionics 179 (2008) 924.
[9] Y. Liu, Y.J. Wang, L.L. Xiao, D.W. Song, L.F. Jiao, H.T. Yuan, Electrochem. Commun. 9 (2007) 925.
[10] Q.H. Wang, L.F. Jiao, H.M. Du, D.W. Song, W.X. Peng, Y.J. Wang, et al., Electrochim. Acta 55 (2010) 7199.
[11] Y. Han, Y.J. Wang, Y.P. Wang, L.F. Jiao, H.T. Yuan, Int. J. Hydrogen Energy 35 (2010) 8177.
[12] D.S. Lu, W.S. Li, C.L. Tan, R.H. Zeng, Electrochim. Acta 55 (2009) 171.
[13] D.W. Song, Y.J. Wang, Y.P. Wang, L.F. Jiao, H.T. Yuan, Electrochem. Commun. 10 (2008) 1486.
[14] Y.F. Liu, Y.H. Cao, L. Huang, M.X. Gao, H.G. Pan, J. Alloys Compd. (2010), doi:10.1016/j.jallcom.2010.08.157.
[15] S.Q. Shi, C.R. Li, W.H. Tang, J. Alloys Compd. 476 (2009) 874.
[16] Y. Liu, Y.J. Wang, L.L. Xiao, D.W. Song, L.F. Jiao, H.T. Yuan, Int. J. Hydrogen Energy 32 (2007) 4220.
[17] S.J. Qiu, H.L. Chu, Y. Zhang, Y.N. Qi, L.X. Sun, F. Xu, J. Alloys Compd. 462 (2008) 392.
[18] F. Li, K. Young, T. Ouchi, M.A. Fetcenko, J. Alloys Compd. 471 (2009) 371.
[19] Y. Zhao, M.X. Gao, Y.F. Liu, L. Huang, H.G. Pan, J. Alloys Compd. 496 (2010) 454.
[20] Z.W. Dong, L.Q. Ma, X.D. Shen, L.M. Wang, Y.M. Wu, L.D. Wang, Int. J. Hydrogen Energy (2010), doi:10.1016/j.ijhydene.2010.08.056.
[21] D.W. Song, Y.J. Wang, Q.H. Wang, Y.P. Wang, L.F. Jiao, H.T. Yuan, J. Power Sources 195 (2010) 7115.